

Mobile Teleoperation: Feasibility of Wireless Wearable Sensing of the Operator’s Arm Motion

Guanhao Fu¹, Ehsan Azimi², Peter Kazanzides²

Abstract—Teleoperation platforms often require the user to be situated at a fixed location to both visualize and control the movement of the robot and thus do not provide the operator with much mobility. One example is in existing robotic surgery solutions that require the surgeons to be away from the patient, attached to consoles where their heads must be fixed and their arms can only move in a limited space. This creates a barrier between physicians and patients that does not exist in normal surgery. To address this issue, we propose a mobile telesurgery solution where the surgeons are no longer mechanically limited to control consoles and are able to teleoperate the robots from the patient bedside, using their arms equipped with wireless sensors and viewing the endoscope video via optical see-through head-mounted displays (HMDs). We evaluate the feasibility and efficiency of our user interaction method compared to a standard surgical robotic manipulator via two tasks with different levels of required dexterity. The results indicate that with sufficient training our proposed platform can attain similar efficiency while providing added mobility for the operator.

I. INTRODUCTION

Teleoperation is used in many applications where human presence must be extended to otherwise inaccessible areas, such as remote or dangerous locations (e.g., undersea, in space, or geographically distant) or small spaces (e.g., inside the patient’s body during minimally-invasive surgery). At a minimum, these systems require a master console for the human operator to view camera images of the remote environment and then send motion commands to the remote robot(s). An example of a more complex master console is provided by the da Vinci Surgical System (Intuitive Surgical, Sunnyvale CA) [1], shown in Fig. 1-left, where the primary surgeon sits at the master console, views stereo video on two displays (one for each eye), and controls the position of the remote robotic instruments using two Master Tool Manipulators (MTMs), which are 7 degree-of-freedom (dof) motorized mechanical linkages with an encoded passive gripper. In this scenario, the surgeon is not scrubbed (not sterile) and is located away from the patient, thereby requiring an assistant to be present at the patient bedside.

The da Vinci provides one motivating example for a portable master console, as shown in Fig. 1-right, because it would enable the surgeon to sit at the bedside, scrubbed, and be able to directly interact with the patient when necessary. Clinically, this would enable “solo” surgeries, where the primary surgeon is able to perform the complete procedure, without a bedside assistant. More generally, however, the existence of a portable console would provide advantages in

other telerobotic scenarios, such as disaster response, bomb disposal, or remote assistance for the disabled or elderly.

A head-mounted display (HMD) provides an obvious component for a portable master console, as it enables visualization of the remote environment. Modern HMDs also include sophisticated sensing, such as multiple cameras and depth sensors, and recent advances in hand tracking have enabled natural gesture-based interactions. However, at present, it is not clear that HMD-based hand tracking would be sufficiently robust for high-precision tasks, such as surgery, and whether the requirement to keep the hands in the field-of-view of the HMD sensors would be comfortable for the operator. For example, a recent study used the HoloLens sensors to detect fine movements of the hands and fingers as well as touch interaction [2], but this method requires a line of sight to the hand and can introduce uncertainty.

We therefore propose the use of body-mounted inertial measurement units (IMUs) to provide the motion input for controlling the remote robots. We note that teleoperation interfaces may require the operator to specify more than the 6 dof positions of the remote robots. For example, in the da Vinci example cited above, it is also necessary to actuate the robotic instrument (e.g., open or close the jaws). We do not address this requirement here but, depending on the application, these additional actions could be implemented in a number of ways, including voice command, foot pedal, myoelectric sensing, or via a hand-held wireless device. At the same time, in order to have real mobility, a teleoperation system should be co-located anytime anywhere with the surgeon and therefore a wearable form factor is devised. Other lightweight setups, such as Phantom Omni, do not provide the mobility or portability of a wearable as they still must be fixed to a base and are merely a smaller MTM.

Related work includes a hand-held device, developed by Steidle et al. [3], that was tracked by fusion of optical and inertial sensing. The advantage of this approach is that it can provide measurements to drive both the position and actuation of the instrument, especially since the hand-held device can be designed with an appropriate interface mechanism. One significant disadvantage, however, is the weight of the hand-held device, which can cause fatigue during prolonged use. In addition, the tracking technology may not be sufficiently reliable for critical tasks such as surgery. Their system fused optical and inertial sensing, which can suffer from obstruction of the line-of-sight and intermittent erroneous readings (e.g., due to computer vision failures), which can only be compensated by the inertial sensing for brief periods of time. Electromagnetic tracking would avoid the line-of-

¹ Dept. of Mechanical Engineering, ² Dept. of Computer Science, Johns Hopkins University, Baltimore USA, pkaz@jhu.edu

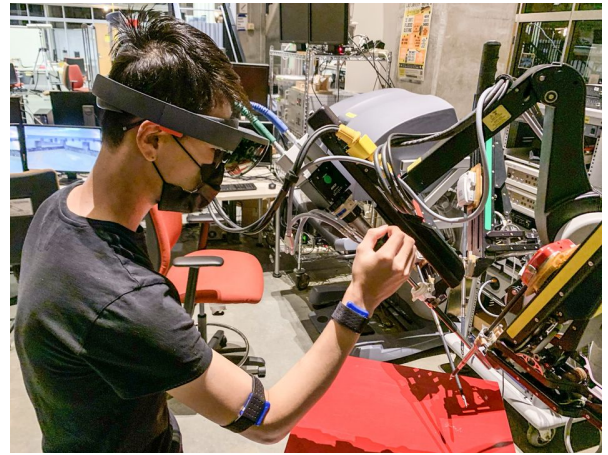


Fig. 1. **Left:** Current teleoperation system where user is fixed to console and situated away from the robot. **Right:** Proposed mobile teleoperation system where user wears stereoscopic see-through HMD, situated next to the robot and operates the robot using a wearable motion capture system.

sight constraint, but be susceptible to electromagnetic field distortion. Another disadvantage is that the operator would need to put down the hand-held device to perform other tasks, and then have to pick it up again to continue teleoperation.

In addition, an IMU-based teleoperation system was introduced in [4]; however, that work focused on using human arm motion to resolve the kinematic redundancy of a 7 degree-of-freedom robot and their experiments did not demonstrate the precise operation that would be required for surgical tasks.

This paper first presents our system design in Section II, including the kinematics of the IMU sensing system and a method for calibrating the link lengths of the human arm. Section III then describes the experimental setup to evaluate calibration accuracy, followed by experiments that compare the proposed IMU-based system to a da Vinci Master Tool Manipulator (MTM) to teleoperate virtual objects in two simulated training tasks. The results of those evaluations and comparative studies are presented in Section IV, followed by the discussion and conclusions in Section V.

II. SYSTEM DESCRIPTION

We propose an alternative master console to teleoperate robotic devices that uses IMUs as the input devices and Microsoft HoloLens as the visualization device. Ultimately, we envision a 6 IMU system that has 3 IMUs for each arm of the user, which provides 6 dof Cartesian space control of robotic devices. Additionally, robotic instrument actuation will be addressed by a hand-held gripper device.

In this paper, we use 2 IMUs to achieve Cartesian space control of a virtual object, where the position and orientation of the virtual object reflect the user's wrist pose. In the next iteration, a third IMU will be included so that our system can account for the 2 dof at the human wrist, which are wrist abduction/adduction, and wrist flexion/extension.

Based on our prior experience with inertial sensing [5]–[7], we realize that it is challenging to obtain accurate orientation. First, all inertial sensors (accelerometer, gyroscope, magnetometer) are subject to drift. Second, while a magnetometer (digital compass) provides an absolute measurement of

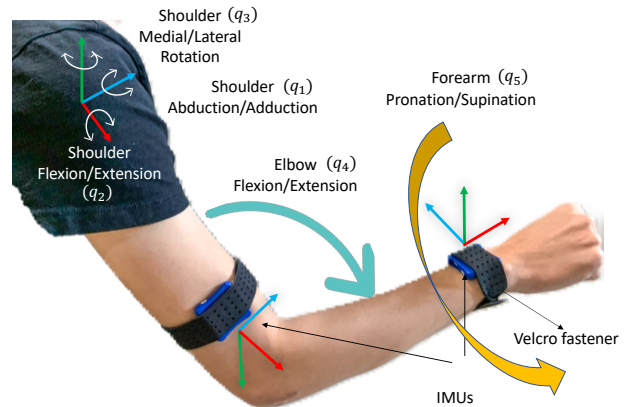


Fig. 2. Experimental Setup: Two wireless IMUs are attached to the upper arm and the forearm

heading, it is subject to magnetic field distortion. The alternative is to integrate the gyroscope reading, which is inaccurate due to drift (bias). In this particular application, however, the operator is controlling the position of a remote robotic end-effector with real-time visual feedback of the end-effector position. We hypothesize that this human visual-feedback loop would be tolerant of measurement drift because it would compensate for the induced error. The goal of our experiments is to provide evidence to support this hypothesis.

A. IMU System Kinematic Model

The two IMUs (LPMS-B2, LP-RESEARCH Inc., Japan) are strapped onto the user's forearm and upper-arm (see Fig. 2), and the orientation outputs after fusing the raw data from accelerometer and gyroscope are used to obtain the end-effector position and orientation. Since there are 2 IMUs, this system is capable of capturing 5 dof based on a simplified human arm kinematic model [8], which includes shoulder abduction/adduction (q_1), shoulder flexion/extension (q_2), shoulder medial/lateral rotation (q_3), elbow flexion/extension (q_4), and forearm pronation/supination (q_5).

In the proposed system, however, joint angles are not directly measured by the IMU and the remote robot kinematics

do not match the human arm kinematics, so only arm pose in Cartesian space is required. Thus, a simplified ball joint representation of the human arm is introduced instead, as shown in Fig. 3. The shoulder joint has 3 dof: q_1 , q_2 , and q_3 , and the elbow joint has 2 dof: q_4 and q_5 .

The position and orientation of the user's wrist, $T_{wp} = F[R_{wp}, p_{wp}]$ w.r.t. the world coordinate frame is given by:

$$T_{wp} = F[R_s, p_s] \cdot F[R_e, p_e] \cdot F[R_w, p_w] \quad (1)$$

where $R_s = R_1$, $R_e = R_1^{-1} \cdot R_2$, and R_w is an identity rotation (see Fig. 3 for frame definitions). Here, $p_s = [0, 0, 0]^T$, since we assume the center of the shoulder joint is aligned with the world coordinate's origin. R_1 and R_2 are the orientation of IMU 1 and IMU 2 w.r.t. the world coordinate frame. We also assume that the IMUs are aligned with the axes of the upper-arm and forearm which requires careful alignment in our experiments; if necessary, existing calibration methods, such as [9], can be used to compensate for any misalignment.

Here, the user's upper-arm and forearm lengths, l_u and l_f , are needed to compute the user's wrist pose:

$$p_e = [l_u, 0, 0]^T \quad p_w = [l_f, 0, 0]^T \quad (2)$$

The values of l_u and l_f can be obtained by the calibration procedure described in the next section or by physical measurement of the operator's arm link lengths.

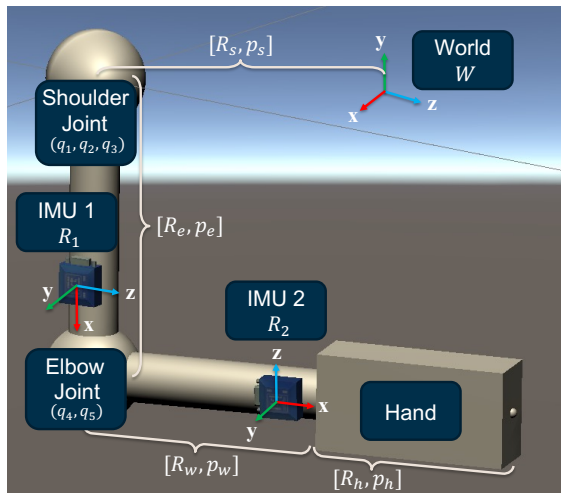


Fig. 3. Simplified ball joint representation of human arm

B. User's Arm Length Calibration

The developed calibration method requires users to touch at least 4 of the 9 different points shown in Fig. 4, which can be printed or shown on any flat surface, as long as the physical distances between the points can be accurately measured. Users should not rotate their hip or torso during the calibration procedure because the current 2 IMU system assumes that the user's shoulder joint is fixed in position and orientation. More importantly, the user needs to touch different points with fully extended index finger, and without rotating the wrist, then record the orientation of the 2 IMUs R_1 and

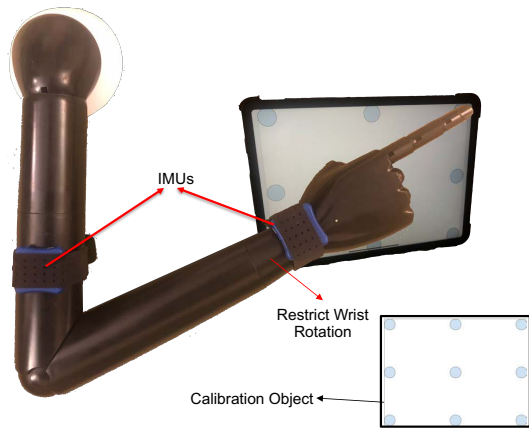


Fig. 4. Calibration setup using mannequin arm

R_2 at each calibration point on the object. The reason that we chose to use the user's extended index finger is because it is a relatively intuitive way for users to touch designated points on an object. We extend Eq. (1) to include the hand and fingertip as follows:

$$T_{ft} = F[R_s, p_s] \cdot F[R_e, p_e] \cdot F[R_w, p_w] \cdot F[R_h, p_h] \quad (3)$$

$$p_h = [l_h, 0, 0]^T \quad (4)$$

$T_{ft} = F[R_{ft}, p_{ft}]$ is the position and orientation of the user's fingertip w.r.t. the world frame and p_h is the user's hand length measured from the wrist. R_h is an identity rotation because wrist rotation is restricted during the calibration and we use a measured value of 0.2 m for l_h .

When the user touches a calibration point i on the calibration object, the fingertip position $p_{ft}(i)$ is recorded. Then, we compute the distance between where the user's fingertip touches points i and j , where $i \neq j$, and denote it as the distance from the forward kinematics: d_{FK} .

$$d_{FK}(i, j) = |p_{ft}(i) - p_{ft}(j)|, i \neq j, i, j \in [1, 2, \dots, 9] \quad (5)$$

Similarly, we denote the true physical distance between the same two calibration points as:

$$d_{tr}(i, j) = |p_{tr}(i) - p_{tr}(j)|, i \neq j, i, j \in [1, 2, \dots, 9] \quad (6)$$

We use the Matlab `fmincon` optimizer to find the l_u and l_f that minimizes:

$$\sum_{i,j} \|d_{FK}(i, j) - d_{tr}(i, j)\| \quad (7)$$

III. EXPERIMENTS

The following sections present the experiments performed to evaluate the calibration accuracy and teleoperation performance of our IMU-based system.

A. Calibration Accuracy

To evaluate our calibration method, we mounted the IMUs on a mannequin arm and manually moved the arm to touch 4 of the 9 calibration posts shown in Fig. 4. We used a mannequin arm because accurate measurement on a human

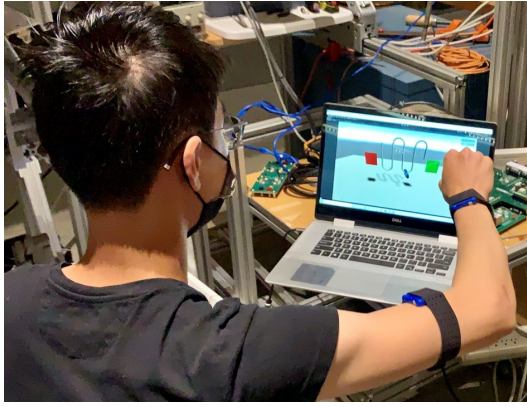


Fig. 5. Experimental setup: User performing the curved wire task using proposed system (Left) and the straight wire task using da Vinci MTM (Right)

arm is challenging due to skin artifact introducing unwanted IMU movement [9]–[11]. It is also difficult to obtain accurate ground-truth measurements of human arm lengths.

B. Teleoperation Performance

After calibrating the user’s arm lengths, we evaluate the performance of our system compared to the MTM from the da Vinci Research Kit (dVRK), an open source research platform based on the first-generation da Vinci surgical robot [12], as seen in Fig. 5.

To capture the performance of our proposed system, we designed two tasks with different levels of required dexterity. We measured both accuracy in position and orientation as well as task completion time.

1) *Visualization Setup*: We designed the tasks around a classic steady-hand game that can often be found in surgical robotics training curricula [13]. The tasks consist of two main objects, a ring and a wire, and the user is required to move the ring along the wire without any collision (see accompanying video). The tasks are visualized in Unity3D, with intuitive start and stop buttons that automatically record time stamped data to evaluate position and orientation accuracy. As shown in Fig. 7, there is also a simultaneous view of the above mentioned simplified ball joint representation of the user’s arm configuration. It is important to note that the visualization is in 2D, with a slight pan angle for improved depth perception.

In Fig. 6, the wire is straight and is horizontally oriented. In Fig. 7, the wire is S-shaped, which requires a higher level of dexterity, thus serving as a good evaluation of our system’s ability to perform more complex tasks. In both task setups, the wires have 25 mm diameter, and the rings have 60 mm inner diameter (ID) and 100 mm outer diameter (OD), which makes the collision threshold 17.5 mm. The wire shape dimensions are shown in their respective figures.

2) *Input Devices Setup*: We interfaced the IMUs with Unity3D using the Unity plugin developed by LP-RESEARCH Inc. In addition, we streamed the Cartesian position and orientation of the MTM through User Datagram Protocol (UDP) and then converted from a right handed coordinate system to the left handed coordinate system used by Unity3D. We let both input devices directly control the

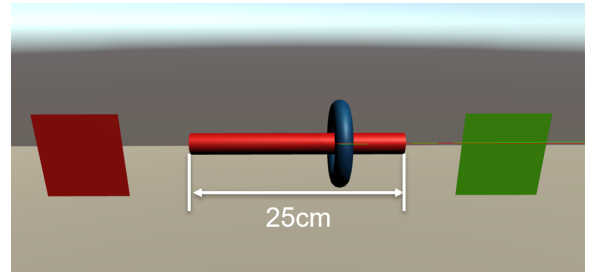


Fig. 6. Unity scene setup: Steady hand task with straight wire

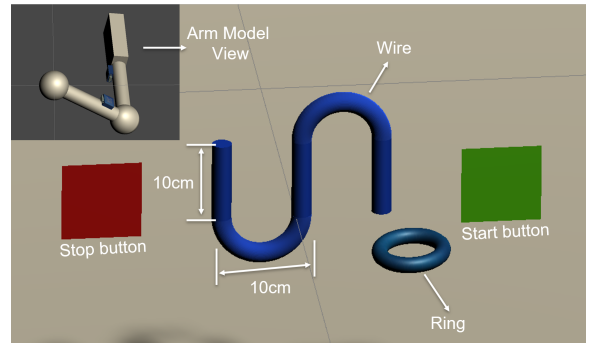


Fig. 7. Unity scene setup: Steady hand task with S-shaped wire

ring object in Unity, without any medium such as grippers used by the da Vinci surgical robot.

IV. RESULTS

A. Calibration Results

We performed 10 trials using our calibration method, where we manually moved the mannequin arm to touch 4 of the 9 calibration posts shown in Fig. 4. Table I shows the errors in the estimated arm lengths, including the average and standard deviation.

B. Teleoperation results

Two users performed each task three times. User1 was familiar with the IMU system, but had no prior experience with the MTM, while User2 was a novice with the IMU but had some experience with the MTM. We evaluated the position and orientation accuracy [14] of both our system and the dVRK while performing the two tasks described above.

TABLE I
CALIBRATION RESULTS: LINK LENGTH ERRORS AS PERCENTAGES OF THE TRUE LENGTHS

	Upper arm	Forearm
Trial 1	3.1%	11.3%
Trial 2	0.9%	4.7%
Trial 3	24.6%	7.7%
Trial 4	14.4%	15.5%
Trial 5	21.7%	6.0%
Trial 6	1.6%	11.5%
Trial 7	0.6%	4.4%
Trial 8	2.1%	0.3%
Trial 9	9.1%	0.2%
Trial 10	18.7%	16.4%
Mean	9.7%	7.8%
Std Dev.	9.4%	5.7%

The position accuracy, at each point on the motion trajectory, is defined as the distance between c_{ring} and c_{wire} :

$$distance(c_{wire}, c_{ring}) \quad (8)$$

where c_{ring} is the ring center, and c_{wire} is the point on the wire center-line that is closest to c_{ring} . The orientation accuracy is defined as the angle between the ring orientation \vec{v}_{ring} and the wire tangent line \vec{v}_{wire} :

$$\alpha = \cos^{-1} \left(\frac{\vec{v}_{wire} \cdot \vec{v}_{ring}}{\|\vec{v}_{wire}\| \cdot \|\vec{v}_{ring}\|} \right) \quad (9)$$

The variation for position and orientation errors with time are presented only for the straight line task for User1 in Fig. 8, due to space limitations. The results for both tasks performed by both users are summarized in Fig. 9. Task completion times for the straight wire and S-shaped wire are provided in Table II. The result shows that it took longer for User2 to complete the task. Table III and Table IV depict the mean position and orientation error for the tasks.

When comparing the performance for the same task and the same user across different input devices, as represented in Fig. 9 and Tables III and IV, we observe that User1, who is more familiar with the system, performs similarly with both systems. This suggests that the proposed IMU system could have comparable position accuracy to the MTM, once

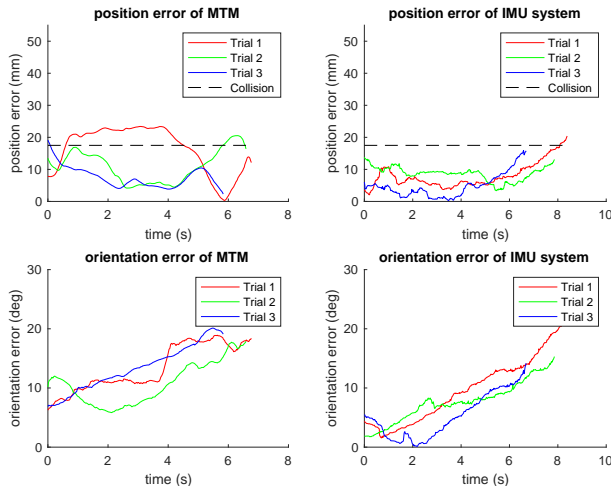


Fig. 8. Result of straight wire teleoperation task for User1

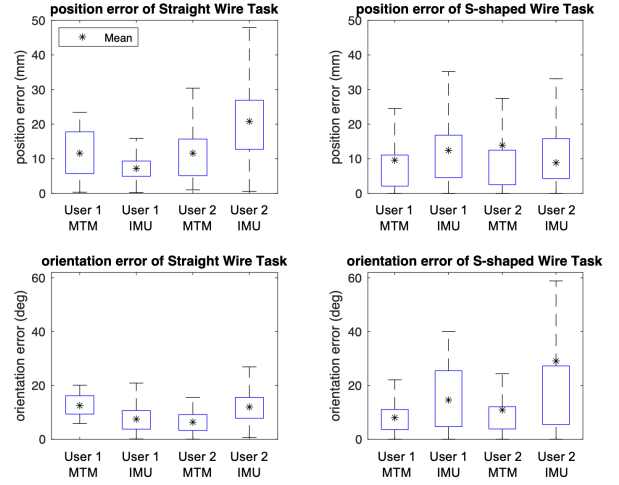


Fig. 9. Accuracy comparison of both users performing two tasks

TABLE II
COMPLETION TIMES FOR TASKS, IN SECONDS

	User1 Trials				User2 Trials			
	1	2	3	Mean	1	2	3	Mean
<i>Straight Wire Task</i>								
MTM	6.8	6.6	5.8	6.4	9.6	11.1	8.4	9.7
IMU	8.4	7.9	6.7	7.6	7.2	9.6	10.8	9.2
<i>S-shaped Wire Task</i>								
MTM	19.7	18.1	16.2	18.0	24.6	22.0	21.1	22.5
IMU	26.6	26.5	21.0	24.7	25.2	28.4	23.8	25.8

the learning curve is completed. For the orientation error, especially while the users were doing the S-shaped wire task, the IMU system has larger errors, which is due to the limited dexterity in the system: our IMU system only captures 5 dof, whereas the MTM has 7 dof. Dashed lines in Fig. 8 represent the threshold where the ring collides with the wire and Table V shows the “success rate” measure, which is the percentage of time that the ring did not collide with the wire.

V. DISCUSSION AND CONCLUSIONS

Table I shows that, on average, the calibration method can estimate the link lengths within 10% of the true values.

TABLE III
MEAN POSITION ERRORS FOR TASKS, IN MILLIMETERS

	User1 Trials				User2 Trials			
	1	2	3	Mean	1	2	3	Mean
<i>Straight Wire Task</i>								
MTM	16.3	11.0	7.6	11.6	11.0	7.0	16.8	11.6
IMU	8.1	8.7	4.8	7.2	27.7	14.9	19.7	20.8
<i>S-shaped Wire Task</i>								
MTM	9.7	10.8	8.2	9.6	16.1	12.8	12.8	13.9
IMU	9.4	10.2	17.6	12.4	9.1	9.9	7.5	8.8

TABLE IV
MEAN ORIENTATION ERRORS FOR TASKS, IN DEGREES

	User1 Trials				User2 Trials			
	1	2	3	Mean	1	2	3	Mean
<i>Straight Wire Task</i>								
MTM	13.4	10.7	13.3	12.5	6.5	5.9	6.7	6.4
IMU	9.6	7.7	5.2	7.5	12.7	11.4	11.8	12.0
<i>S-shaped Wire Task</i>								
MTM	6.5	6.9	10.7	8.0	10.6	10.9	11.3	10.9
IMU	13.7	14.8	15.3	14.6	30.8	28.3	28.1	29.1

TABLE V
NON-COLLISION PERCENTAGE FOR STRAIGHT WIRE TASK

	User1	User2
MTM	74.5%	85.8%
IMU	98.7%	47.4%

However, this table also shows significant variation in the result, even though each trial was performed with the calibration object in approximately the same location. Better repeatability could possibly be obtained by using more than 4 calibration points, at the cost of a longer calibration time. From the results of the teleoperation experiments, however, we can conclude that the current calibration accuracy is sufficient for the evaluated tasks because performance was comparable to a conventional input device, with differences that could be attributed to user familiarity.

Table V indicates that despite the inherent challenges with IMUs, a trained user can perform the task with a high success rate. For a novice user, performance with the MTM was generally better than with the IMU. Of course, participants using IMU input were limited by the range of motion of human arms and by the boundaries of their workspace. One possible way to address this issue is to introduce a clutch input so that when users reach the workspace limit, they can clutch and reorient themselves in a neutral location to have room to continue the task.

Limitations of this feasibility study include the small number of participants (two), limited trials per task (three), and differences in participant experience and possible effect of a learning curve. Furthermore, this study did not quantify the IMU sensor drift, so it is uncertain how much visual compensation was required.

While the IMU-based system provided comparable performance to the MTM in terms of allowing the user to specify motion of the remote object, unlike the mechanically-grounded MTM, it cannot provide haptic feedback. One possible solution is to add vibrotactile actuators, for example, on the IMUs. Other possible solutions include sensory substitution (e.g., graphical overlays [15] or audio cues [16], [17] to indicate measured force) or force feedback to some other part of the body, such as the forearm or wrist [18].

In summary, this study evaluated the feasibility of mobile teleoperation using wireless IMUs mounted on the user's arm by comparing the efficiency of the system against a standard mechanical input device used for robotic surgery. The results show that our proposed solution is a trade-off that adds considerable mobility while introducing some inaccuracy, though the inaccuracy may be mitigated by user training and stereoscopic visualization. This study provides evidence that although an IMU-based input device is subject to drift, it can effectively be used in teleoperation scenarios where the operator is closing the control loop based on visual feedback. We are currently integrating the IMU-based system with a HoloLens HMD to provide a complete teleoperation solution. Stereoscopic visualization provided by the HMD can potentially mitigate the errors caused by a lack of sufficient depth perception in our current visualization. We also intend

to add a clutch function to address the workspace limitation and to conduct a controlled multi-user study.

ACKNOWLEDGMENTS

Anton Deguet assisted with the system integration.

REFERENCES

- [1] G. Guthart and J. K. Salisbury Jr, "The Intuitive™ telesurgery system: Overview and application." in *IEEE Intl. Conf. on Robotics and Automation (ICRA)*, 2000, pp. 618–621.
- [2] R. Xiao, J. Schwarz, N. Throm, A. D. Wilson, and H. Benko, "MRTouch: Adding touch input to head-mounted mixed reality." *IEEE Trans. on Vis. & Comp. Graphics*, vol. 24, no. 4, pp. 1653–1660, 2018.
- [3] F. Steidle, A. Tobergte, and A. Albu-Schäffer, "Optical-inertial tracking of an input device for real-time robot control," in *IEEE Intl. Conf. on Robotics and Automation (ICRA)*, May 2016, pp. 742–749.
- [4] A. Nocco, F. Cordella, L. Zollo, G. Di Pino, E. Guglielmelli, and D. Formica, "A teleoperated control approach for anthropomorphic manipulator using magneto-inertial sensors," in *IEEE Intl. Symp. on Robot and Human Interactive Comm. (RO-MAN)*, 2017, pp. 156–161.
- [5] H. Ren, D. Rank, M. Merdes, J. Stallkamp, and P. Kazanzides, "Multisensor data fusion in an integrated tracking system for endoscopic surgery," *IEEE Trans. on Info. Tech. in Biomed.*, vol. 16, no. 1, pp. 106–111, Jan 2012.
- [6] H. Ren and P. Kazanzides, "Investigation of attitude tracking using an integrated inertial and magnetic navigation system for hand-held surgical instruments," *IEEE/ASME Trans. on Mechatronics*, vol. 17, no. 2, pp. 210–217, Apr 2012.
- [7] C. He, P. Kazanzides, H. T. Sen, S. Kim, and Y. Liu, "An inertial and optical sensor fusion approach for six degree-of-freedom pose estimation," *Sensors*, vol. 15, no. 7, pp. 16448–16465, Jul 2015.
- [8] A. Bertomeu-Motos, A. Blanco, F. J. Badesa, J. A. Barrios, L. Zollo, and N. Garcia-Aracil, "Human arm joints reconstruction algorithm in rehabilitation therapies assisted by end-effector robotic devices," *J. of NeuroEngin. & Rehab.*, vol. 15, no. 1, pp. 1–11, 2018.
- [9] P. Mueller, M.-A. Begin, T. Schauer, and T. Seel, "Alignment-free, self-calibrating elbow angles measurement using inertial sensors," *IEEE J. of Biomedical & Health Info.*, vol. 21, no. 2, pp. 312–319, 2017.
- [10] I. H. Lopez-Nava and M. M. Angelica, "Wearable Inertial Sensors for Human Motion Analysis: A review," *IEEE Sensors Journal*, vol. 16, no. 22, pp. 7821–7834, 2016.
- [11] M. El-Gohary and J. McNames, "Shoulder and elbow joint angle tracking with inertial sensors," *IEEE Transactions on Biomedical Engineering*, vol. 59, no. 9, pp. 2635–2641, 2012.
- [12] P. Kazanzides, Z. Chen, A. Deguet, G. S. Fischer, R. H. Taylor, and S. P. DiMaio, "An open-source research kit for the da Vinci® surgical system," in *IEEE Intl. Conf. on Robotics and Automation (ICRA)*, Hong Kong, China, Jun 2014, pp. 6434–6439.
- [13] A. Mariani, E. Pellegrini, N. Enayati, P. Kazanzides, M. Vidotto, and E. De Momi, "Design and Evaluation of a Performance-based Adaptive Curriculum for Robotic Surgical Training: A Pilot Study," in *IEEE Engin. in Medicine and Biology Conf. (EMBC)*, 2018, pp. 2162–2165.
- [14] N. Enayati, A. M. Okamura, A. Mariani, E. Pellegrini, M. M. Coad, G. Ferrigno, and E. De Momi, "Robotic assistance-as-needed for enhanced visuomotor learning in surgical robotics training: An experimental study," in *IEEE Intl. Conf. on Robotics and Automation (ICRA)*, 2018, pp. 6631–6636.
- [15] T. Akinbiyi, C. E. Reiley, S. Saha, D. Burschka, C. J. Hasser, D. D. Yuh, and A. M. Okamura, "Dynamic augmented reality for sensory substitution in robot-assisted surgical systems," in *IEEE Engin. in Medicine and Biology Conf. (EMBC)*, 2006, pp. 567–570.
- [16] M. Balicki, A. Uneri, I. Iordachita, J. Handa, P. Gehler, and R. Taylor, "Micro-force sensing in robot assisted membrane peeling for vitreoretinal surgery," in *Medical Image Computing and Computer-Assisted Intervention (MICCAI)*, 2010, pp. 303–310.
- [17] N. Cutler, M. Balicki, M. Finkelstein, J. Wang, P. Gehler, J. McGready, I. Iordachita, R. Taylor, and J. T. Handa, "Auditory force feedback substitution improves surgical precision during simulated ophthalmic surgery," *Investigative Ophthalmology & Visual Science*, vol. 54, no. 2, pp. 1316–1324, Feb. 2013.
- [18] G. Ng, P. Barralon, G. Dumont, S. K. W. Schwarz, and J. M. Ansermino, "Optimizing the tactile display of physiological information: Vibrotactile vs. electro-tactile stimulation, and forearm or wrist location," in *IEEE Engin. in Med. and Bio. Conf. (EMBC)*, 2007, pp. 4202–4205.